M&C 2017 - International Conference on Mathematics & Computational Methods Applied to Nuclear Science & Engineering, Jeju, Korea, April 16-20, 2017, on USB (2017)

Spectral Rehomogenization of Nodal Cross-Sections via Proper Orthogonal Decomposition

M. Gamarino*, A. Dall'Osso†, D. Lathouwers*, J.L. Kloosterman*

**Department of Radiation, Science and Technology, Delft University of Technology, Mekelweg 15, 2629 JB Delft, The Netherlands*
†AREVA NP, Tour AREVA, 92084 Paris La Défense Cedex, France
M.Gamarino@tudelft.nl

Abstract - *Industrial reactor-core calculations mostly resort to the nodal-diffusion methodology, relying on the homogenization paradigm for the generation of few-group assembly cross-sections. The incapability of cross-sections condensed with the infinite-medium spectrum to model core-environment spectral effects is one of the major limitations in the numerical simulation of current- and next-generation reactor cores, characterized by strongly heterogeneous geometrical layouts. AREVA NP has recently proposed a spectral-correction method to reproduce the variation of the neutron spectrum between environmental and infinite-lattice conditions by means of a modal expansion approach, which is solved for by Galerkin or Petrov-Galerkin projection of the local fine-group neutron balance equation over a set of weighting operators. The accuracy of this method significantly depends on the choice of the basis and test functions. Purely analytical modes turn out to be often inadequate to reproduce the strongly varying shape of the spectrum deformation in the reactor core. The present paper investigates an alternative strategy building upon the Proper Orthogonal Decomposition (POD). This approach relies on the calculation of the optimal (in a least-square sense) orthonormal basis functions for the space spanned by a set of snapshots of the reference spectrum variation. In our work, we test the capability of the POD modes to contain characteristics of the spectral interactions between fuel-assemblies in the reactor core. It is shown that the POD-Galerkin-based spectral rehomogenization can reconstruct very accurately the spectrum in the real environment.*

I. INTRODUCTION

Few-group cross-sections used in nodal diffusion codes for 3D reactor core simulations derive from standard energy collapsing and spatial homogenization performed during preliminary lattice transport calculations with reflective boundary conditions [1]. The infinite-medium neutron flux used for cross-section weighting does not account for environmental effects arising in case of heterogeneous core configurations, common examples of which are mixed MOX/UO_2 fuel-loading patterns, reflector boundaries, layouts with depletable strong local absorbers and elaborate insertion schemes of control mechanisms. With these increasingly widespread complex designs reducing the neutron leakage and optimizing the core-power distribution, nodal cross-sections built by the standard homogenization paradigm could fail to reproduce accurate estimates of reaction rates and the multiplication factor. Therefore, core-environment conditions need to be modeled to provide more accurate inputs for nodal solvers.

Environmental effects triggered by core and assembly heterogeneity affect the neutron flux shape in both space and energy. Though spatial and spectral effects are tightly coupled, for sake of simplicity they are usually addressed separately by reactor analysis methods. For example, at AREVA NP a spatial rehomogenization method has been developed [2]. In the present work we focus on spectral aspects. A number of techniques have been proposed in the past to correct single-assembly cross-sections for spectrum effects. One of them applies empirical correlations accounting for local spectral interactions [3]. Recently a spectral rehomogenization method has been developed at AREVA NP [4], as part of a more general cross-section correction model aiming to reproduce environmental effects of various nature [5]. The proposed approach consists of estimating the difference between the environmental and infinite-medium node-average spectra by means of a limited set of known modal components in the domain of energy. The energy-condensation defects are thus evaluated on-the-fly and added to the nodal cross-sections provided by the standard lattice calculation. A similar approach, called recondensation, has been also studied at MIT [6].

A critical point in the definition of a modal expansion method for the spectrum change in the real environment is the choice of a suitable set of basis and test functions. These considerably affect the accuracy of the core-flux energy distribution reconstruction and, hence, of the cross-section update calculation. Modal synthesis methods have been extensively used for reactor physics applications, and several "recipes" can be found in literature for the selection of modes and weighting operators, based on either physical insight as to the nature of the sought solution or purely mathematical considerations [7]. In the original version of the spectral rehomogenization model [4], the basis functions were chosen to be a combination of mathematical functions (Chebyshev polynomials and exponential functions), together with a physically justified mode (fission spectrum). Step functions were instead taken as weighting modes. Their range was defined by a heuristic procedure, attempting to minimize the deviation of the computed real-environment spectrum from the reference one for some benchmark problems. However, the results of this implementation showed that, despite of the use of the reference-leakage energy distribution as input, for certain assembly configurations the prediction of the spectral deformation caused by the

environment suffers from insufficient accuracy, especially in the fast and epithermal ranges [5]. Here, neutron migration is dominated by inelastic collisions and resonance absorption, which causes the spectrum-variation shape to exhibit a strongly varying and irregular behavior, more difficult to be faithfully reproduced by merely mathematical modes. In order to enhance the effectiveness of the method, an extensive investigation of alternative trial and weighting functions has been carried out. In this work we present a new approach based on the Proper Orthogonal Decomposition (POD), combined with Galerkin projection. The POD is a Reduced Order Modeling (ROM) technique that has been widely used in the last decades in many scientific and engineering fields. It extracts "mode shapes" or basis functions from experimental data or detailed simulations of high-dimensional systems [8]. The resulting modes have the valuable property of inheriting "physical" information about the system of interest and can be used to project the high-order problem into the corresponding reduced subspace [9]. A low-dimension approximate description of the problem under study is thus possible. Though a growing interest in the POD has been recently shown also in the nuclear community, a limited number of works can be found in literature on its applications to reactor modeling problems [10–13].
In this paper, we investigate the feasibility of a POD approach for the search of basis (and test) functions in the framework of our spectral cross-section correction model. This is done by means of numerical simulations of few assembly-configuration samples, representative of the spectral effects of the environment observable in a reactor core. The procedure followed to compute the POD modes, building upon the method of snapshots [14] and the Singular Value Decomposition (SVD) tool [8], is described. The capability of the obtained basis functions to contain characteristics from the phenomenon of interest (i.e., spectral interactions between fuel-assemblies) and to capture relevant information (the "energy" of the system) is analyzed. The results of nodal calculations with POD-based spectrum-corrected cross-sections are compared to reference values from the continuous-energy Monte Carlo neutron transport code SERPENT [15]. In our analysis we point out the main advantages and shortcomings of this approach, in terms of both accuracy and computational effort. Additional ongoing developments are also outlined, in the light of a more extensive application of the proposed methodology in the framework of spectral rehomogenization. These include, for instance, the development of a model for an accurate representation of the neutron leakage energy distribution.

II. THEORY

In this section the main features of the spectral cross-section correction method considered in the present work are summarized, and the underlying ideas of our POD approach are outlined. An overview of the proposed methodology follows. As an exhaustive description of the POD theory is out of the scope of this paper, only the aspects of interest in the context of our work are highlighted. For a complete dissertation on this topic, the interested reader might refer to [9].

1. The Spectral Rehomogenization Model

The neutron energy-balance equation in the real environment can be written, for a generic homogenized node, as [4]:

$$\Sigma_t(E)\Phi_{\text{env}}(E) + L(E) = \frac{\chi(E)}{k_{\text{eff}}}\int_0^\infty dE'\nu\Sigma_f(E')\Phi_{\text{env}}(E') + \int_0^\infty dE'\Sigma_s(E'\rightarrow E)\Phi_{\text{env}}(E'), \quad (1)$$

where $\Phi_{env}(E)$ and $L(E)$ represent respectively the spectrum in environmental conditions and the leakage energy distribution. The meaning of the remaining symbols corresponds to common notation in reactor physics literature. In order to ease the search of basis and test functions, the energy E is replaced by a lethargy-like quantity u, defined separately within each coarse energy-group G as:

$$u = \frac{\ln\left(\frac{E}{E_{mG}}\right)}{\ln\left(\frac{E_{pG}}{E_{mG}}\right)},$$

where E_{pG} and E_{mG} denote the $G-$group upper and lower energy boundaries. The variable u is thus bounded between 0 and 1 in each macro-group. We consider here $N_G = 2$, with $E_{p1} = 19.6$ MeV, $E_{m1} \equiv E_{p2} = 0.625$ eV and $E_{m2} = 1.1 \cdot 10^{-10}$ MeV. Moving to the 2-group framework and replacing E with u, Eq. (1) can be rewritten, for group G, as:

$$\Sigma_{t,G}(u)\Phi_{\text{env},G}(u) + L_G(u) = \sum_{G'=1}^{2}\left(\frac{\chi_G(u)}{k_{\text{eff}}}\cdot\int_0^1 du'\nu\Sigma_{f,G'}(u')\cdot\Phi_{\text{env},G'}(u') + \int_0^1 du'\Sigma_{s,G'\rightarrow G}(u'\rightarrow u)\Phi_{\text{env},G'}(u')\right). \quad (2)$$

In each coarse group, the environmental spectrum is defined as the sum of the reference distribution in infinite-medium conditions (here normalized to the node-average integral flux $\bar{\Phi}_G$ coming from the nodal calculation) and of the sought spectrum variation $\delta\Phi_G(u)$:

$$\Phi_{\text{env},G}(u) = \bar{\Phi}_G\varphi_{\infty,G}(u) + \delta\Phi_G(u). \quad (3)$$

The spectrum difference is expanded in terms of the modal components $Q_{G,i}(u)$, which are the target of our POD analysis:

$$\delta\Phi_G(u) = \sum_{i=1}^{N_{Q_G}}\alpha_{G,i}Q_{G,i}(u). \quad (4)$$

In the current implementation, the number of basis functions N_{Q_G} is set to 4 for both macro-groups. The expansion coefficients $\alpha_{G,i}$ are the unknowns of the spectral rehomogenization problem. In order to solve for them, a standard weighting-residual technique is applied to the lethargy-balance equation: after substitution of Eqs. (3) and (4), Eq. (2) is projected over the test functions $W_{G,j}(u)$ (with $j = 1, ..., N_{Q_G}$) and then integrated over u within each coarse group. For instance, after projection and some manipulation the term corresponding to the total reaction rate reads as follows:

$$\int_0^1 duW_{G,j}(u)\Sigma_{t,G}(u)\Phi_{\text{env},G}(u) = \bar{\Phi}_G h_{R,t,G,j} + \sum_{i=1}^{N_{Q_G}}\alpha_{G,i}h_{V,t,G,i,j}, \quad (5)$$

being the reference ($h_{R,t,G,j}$) and variational ($h_{V,t,G,i,j}$) rehomogenization coefficients respectively defined as:

$$h_{R,t,G,j} = \int_0^1 du W_{G,j}(u)\Sigma_{t,G}(u)\varphi_{\infty,G}(u), \tag{6a}$$

$$h_{V,t,G,i,j} = \int_0^1 du W_{G,j}(u)\Sigma_{t,G}(u)Q_{G,i}(u). \tag{6b}$$

Applying the same procedure to the remaining terms appearing in Eq. (2), the rehomogenization problem can be cast in the following form:

$$\bar{\Phi}_G h_{R,t,G,j} + \sum_{i=1}^{N_{Q_G}} \alpha_{G,i} h_{V,t,G,i,j} + c_{G,j}\bar{L}_G = \sum_{G'=1}^{2} \bar{\Phi}_{G'}\Big(h_{R,s,G'\to G,j} + \frac{\chi_{G,j}}{k_{\text{eff}}} h_{R,f,G'}\Big) + \sum_{G'=1}^{2}\sum_{i=1}^{N_{Q_G}} \alpha_{G',i}\Big(h_{V,s,G'\to G,i,j} + \frac{\chi_{G,j}}{k_{\text{eff}}} h_{V,f,G',i}\Big), \tag{7}$$

where $\bar{L}_G$ is the node-average integral leakage coming from the nodal calculation, whereas $c_{G,j}$, $\chi_{G,j}$ and the coefficients h_R, h_V are the rehomogenization parameters corresponding to the fine-group neutron leakage, fission-emission spectrum and various reaction rates. Variables in Eq. (7) are formulated as follows:

$$c_{G,j} = \int_0^1 du W_{G,j}(u) f_{L,G}(u), \tag{8a}$$

$$\chi_{G,j} = \int_0^1 du W_{G,j}(u)\chi_G(u), \tag{8b}$$

$$h_{R,f,G} = \int_0^1 du\, \nu\Sigma_{f,G}(u)\varphi_{\infty,G}(u), \tag{8c}$$

$$h_{V,f,G,i} = \int_0^1 du\, \nu\Sigma_{f,G}(u)Q_{G,i}(u), \tag{8d}$$

$$h_{R,s,G'\to G,j} = \int_0^1 du W_{G,j}(u) \int_0^1 du'\Sigma_{s,G'\to G}(u'\to u)\varphi_{\infty,G'}(u'), \tag{8e}$$

$$h_{V,s,G'\to G,i,j} = \int_0^1 du W_{G,j}(u) \int_0^1 du'\Sigma_{s,G'\to G}(u'\to u)Q_{G',i}(u'). \tag{8f}$$

In Eq. (8a), $f_{L,G}(u)$ stands for the leakage energy shape. The above-defined coefficients are computed for a given fuel-assembly at the cross-section library level, so no additional lattice calculation is needed when updating cross-sections throughout the nodal simulation.

Eq. (7) reduces to an 8×8 ($N_G N_{Q_G} \times N_G N_{Q_G}$ in the more general form) linear system that is solved independently for each node following the main nodal calculation. After determining the coefficients $\alpha_{G,i}$, the spectral cross-section correction for reaction type R in a generic node can be computed as follows:

$$\delta\Sigma_{R,G} = \frac{1}{\bar{\Phi}_G}\int_0^1 du\Sigma_{R,G}(u)\delta\Phi_G(u) = \frac{1}{\bar{\Phi}_G}\sum_{i=1}^{N_{Q_G}} \alpha_{G,i} h_{V,R,G,i,0}, \tag{9}$$

where the subscript 0 in $h_{V,R,G,i,0}$ means that the weighting function is $W_{G,0}(u) = 1$.

Cross-section distributions used in Eqs. (6) and (8) are, in practice, those of the infinite medium. This is an approximation, as Eq. (1) is rigorously valid in the real environment, where fine-group cross-sections can be influenced by self-shielding effects. However, the analysis performed for the validation of the method revealed that the impact of such approximation is negligible. A limitation of the current implementation is rather that energy-space cross-terms are neglected: the estimated cross-section correction is indeed averaged over the node, whereas in reality the magnitude of spectral effects is significantly higher at the interface with neighbor assemblies.

In order for this model to be applicable, the definition of a suitable energy distribution $f_{L,G}(u)$ for the neutron leakage is required. In most of the present work, the best-estimate shape is taken as input from the reference transport calculation. This allows us to keep the validation of the methodology unaffected by the inaccuracy unavoidably introduced adopting a leakage shape other than the theoretical one. It is thereby possible to focus on the effect of the POD approach on the solution of the nodal calculation with rehomogenized cross-sections.

2. The POD Approach

As mentioned in the introduction, we build our set of POD basis functions $Q^{POD}_{G,i}(u)$ by the method of snapshots, in combination with the Singular Value Decomposition (SVD).

A. The Method of Snapshots and SVD

Generally speaking, a snapshot is the solution of the equation modeling the problem of interest for a specific configuration or state of the system [14]. Each combination of parameters governing the phenomenon under study generates a different state, and can thus be used to obtain a snapshot. In time-dependent problems, snapshots can also be taken as the solution of the dynamically evolving system at given time instances [11]. The snapshots derived from multiple solutions of the high-dimensional problem are collected in an array (the snapshot matrix), which is the input of the SVD [8, 9]. Such factorization of the snapshot matrix returns, among other arrays, a set of orthonormal vectors. It can be proved that these are the optimal (in a least-square sense) orthonormal basis functions for the vector space encompassed by the input matrix. They are referred to as *proper orthogonal modes*, and they are the sought POD basis. The shape of such functions is determined by the information carried within the retained snapshots, and can thus capture some relevant properties of the system under study. Obviously, the higher the number of snapshots, the more comprehensive the amount of information (and, hence, the more successful are the computed modes to catch the overall "energy" and the dynamics of the system). The maximum number of snapshots is mostly dictated by the computational burden associated to their calculation. In the light of these considerations, it is apparent that the POD basis can be built so as to reproduce specific configurations by including their solution in the snapshot series. Moreover, a clever choice of the snapshot set can boost their capability to reproduce the solution of "unseen" problems as well.

B. Application to the Spectral Problem

In the framework of our work, snapshots of the spectrum variation between environmental and infinite-medium conditions are taken. As already mentioned, spectral effects observable in a reactor core mostly take place at the interface between adjacent assemblies. Hence, the main idea of the proposed approach is to model several assembly-interface types for the generation of snapshots. Two-dimensional colorset domains are a suitable candidate for this purpose. This choice has also the advantage of allowing us to decompose the whole-core problem into several sub-problems and, thus, to simplify our analysis. In order to build a set of POD basis being as "energetic" as possible, a separate calculation should be performed for each interface-type in a reactor (i.e., for each unique set of four assemblies). When considering several fuel-loading patterns and assembly shuffling, this would result in a significant computational burden. Moreover, there are other variables which might have an influence on spectrum effects and, thus, need to be accounted for in the snapshot generation process. These include the state parameters describing the thermal-hydraulic condition of the reactor environment (burn-up, moderator temperature and density, fuel temperature, diluted-boron concentration, etc.). The high-dimensionality of the problem can thus make the snapshot phase very demanding. Despite the repeated evaluations of the problem for the POD-basis calculation have to be performed only once, an effective sampling strategy has to be developed to reduce the amount of costly computations. These aspects are discussed in Section III, where the procedure adopted in this work for the selection of snapshots is outlined.
We generate snapshots by solving the neutron transport equation for the colorset and single-assembly configurations: the environmental and infinite-medium spatially-averaged spectra are thus computed for each fuel bundle, together with the corresponding variation. In order to determine the detailed spectrum change, the number of fine energy-groups g used in the fast and thermal coarse-groups ($G = 1$ and $G = 2$) is respectively 247 and 34. For both macro-groups, the matrix of snapshots A_G is obtained using the spectrum-variation determined for different solutions of the transport problem. The SVD of A_G returns the following matrix decomposition:

$$A_G = U_G S_G V_G^T, \tag{10}$$

where S_G is a diagonal matrix of size $n_G \times N_s$ (being n_G the number of fine groups for the coarse group G and N_s the number of snapshots), whereas U_G and V_G have dimensions $n_G \times n_G$ and $N_s \times N_s$, respectively. The columns of the matrix U_G are the proper orthonormal modes. The elements of S_G, which are non-negative and sorted in descending order, are the singular values of A_G. They are proportional to the "energy" of each mode, that is, its importance in the modal approximation of the vector space spanned by A_G. If all the n_G eigenvectors produced by the SVD are used, the error in the approximation of the original snapshot data goes to 0. The POD basis set, consisting of N_{Q_G} modes, is built from a reduced form of Eq. (10), taking the first N_{Q_G} columns of U_G. The corresponding array provides a modal approximation of the snapshot set which minimizes the error in the L_2-norm compared to all the other approximations. As stated in Section II.1, in our spectral rehomogenization method we set N_{Q_G}=4 for both groups. This number of modes is chosen so as to be comparable with the original approach [4, 5]. Moreover, the achieved POD modes are also used as weighting functions (Galerkin weighting).

3. Overview of the Methodology

A flow chart of the global procedure followed in our work is depicted in Figure 1.

The methodology can be split into 2 phases:

- An off-line phase, in which snapshots of the spectrum deformation in the colorset environment are collected for several sample assembly-configurations. These snapshots are used to extract, via the SVD, the set of POD basis with which the rehomogenization parameters are to be computed (by Eqs. (6) and (8)) during the cross-section library preparation.
- An on-line phase, consisting of the actual core calculation. The nodal problem is first solved using the infinite-medium cross-sections interpolated from libraries at the current values of the state parameters for each node. The nodal information (global flux and power distributions, k_{eff}) is then exploited to solve for each assembly the spectral rehomogenization problem and the thermal-feedback calculation. After interpolation from the parameterized tables at the new values of the state parameters, cross-sections can thus be updated with the spectral correction computed by the POD-based rehomogenization.

As for the on-line phase, it is remarked that iterations between the nodal calculation and the spectral rehomogenization problem are nested in the thermal-feedback updates. Therefore, their cost is amortized. Furthermore, the spectral-correction method (which is, as seen in Section II.1, computationally inexpensive) is applied locally for each node. This makes it easily parallelizable. Our methodology is consistent with the two-step procedure commonly adopted in light-water-reactor analysis, in which highly demanding branch transport calculations for the preparation of cross-section libraries (off-line phase) are followed by whole-core calculations with nodal-diffusion solvers (on-line phase).

III. RESULTS AND ANALYSIS

1. Procedure for Validation

For the validation of the proposed method, nodal calculations were performed for three benchmark problems. These were chosen among the most challenging configurations for numerical methods usually encountered in a reactor core, and consist of: a UO_2 colorset with burnable-poison rods (Problem 1); a UO_2 colorset hosting AIC control rods (Problem 2); a UO_2/MOX colorset (Problem 3). Spectral rehomogenization was applied to these test-cases using POD basis (and weighting) functions derived from multiple sets of snapshots:

- snapshots from a single-parameter study for a given interface type (that is, we solved the colorset and single-assembly transport problems sampling different values of a given parameter);

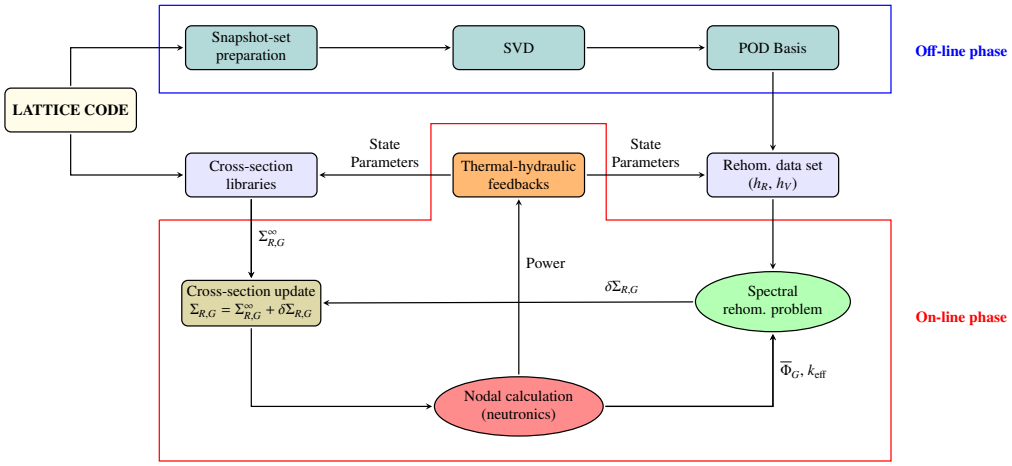

Fig. 1. Flow diagram of the POD-based spectral rehomogenization within the core nodal calculation.

- snapshots from a multi-parameter study for a given interface type;
- assembly of all the snapshots sampled for the three different interface types.

Snapshots were computed via 281-group calculations performed with the continuous-energy Monte Carlo code SERPENT. Each multigroup spectrum-variation solution was obtained running $5.25 \cdot 10^6$ active neutron histories. For reasons related to the computing time, the B_1 critical-spectrum calculation was not performed for the fine-group flux distributions. Nodal simulations were performed with BRISINGR, a TU Delft in-house developed code based on a standard non-linear CMFD-NEM solving strategy. Two-group input cross-sections and discontinuity factors were also computed by SERPENT, which was used as reference for the comparison of the nodal solver outcome. Single-assembly calculations for group-constant generation were run with $5.63 \cdot 10^8$ active neutron histories. A standard deviation lower than 2.5 % was found for all the computed homogenization parameters. Therefore, an uncertainty-propagation analysis was deemed not to be necessary. Simulations were made for fresh initial-core isothermal conditions (i.e., without thermal-hydraulic and fuel-depletion feedacks). The values of the main state parameters correspond to hot full-power conditions (namely, T_{fuel}=846 K, T_{mod}=582 K, p=158 bar). For sake of consistency with the snapshot simulations, no critical-buckling correction was applied. A nodalization of 2×2 nodes per assembly was chosen. For each test-case, three different calculations were performed: with infinite-medium cross-sections from parameterized libraries *(a)*, with cross-sections corrected by means of the reference spectral defect *(b)*, and with POD-based spectral rehomogenization of cross-sections *(c)*. The reference spectral correction was evaluated, according to Eq. (9), by collapsing the fine-group cross-section distribution $\Sigma_{R,G}(u)$ with the reference spectrum variation $\delta\Phi^{ref}_G(u)$ computed in SERPENT. This choice has been done because there are two kinds of errors in cross-section homogenization: spatial and spectral. As only the spectral error is addressed here, the homogenization defect cannot be fully corrected.
The presentation of the results is organized as follows. Focus is first given to the effect of inter-assembly heterogeneity on the calculation of the POD modes and on the performance of spectral rehomogenization. An analysis is then performed on the impact of the state parameters on the POD basis. Finally, some preliminary considerations are made on the ongoing development of a POD-based model for the approximation of the leakage energy distribution.

2. Analysis on Inter-Assembly Heterogeneity

A. Problem 1 - UO_2 Colorset with Pyrex Rods

The 2-D colorset is depicted in Figure 2. It consists of four 17 × 17 PWR fuel assemblies of fresh UO_2 having two different compositions: the former with 1.8% enrichment, the latter with 3.1% enrichment and 16 rods containing burnable absorber (Pyrex). The concentration of diluted boron in the moderator is 700 ppm.

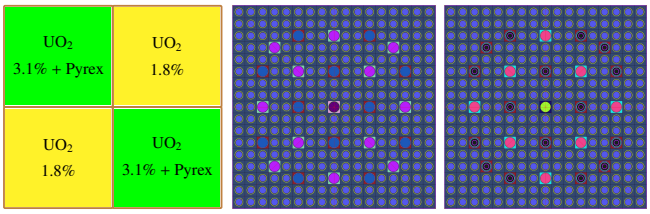

Fig. 2. Assembly set (a) and layout of UO_2 fuel-assemblies with 1.8% enrichment (b) and 3.1% enrichment and Pyrex rods (c).

In this configuration inter-assembly spectral effects are driven by the difference in the enrichment and by the local presence of burnable-poison rods. As the primary goal of this work is to investigate the feasibility of the POD-based rehomogenization, we begin by testing the method with a simple approach for the generation of snapshots. We analyze a one-parameter dependence, with the Pyrex content in the heterogeneous assembly as parametric variable. Solutions for the spectrum

variation were computed sampling uniformly the target range $[5.9 \cdot 10^{-5}, 1.8 \cdot 10^{-3}]$ atoms/cm^3 for the concentration of boron in the burnable-poison rods ($N^{bp}_{B_{10}}$). For validation purposes, an initial number of 200 snapshots was chosen. As a first attempt to analyze the effect of the state parameters on the POD modes, the snapshots were simulated at a diluted-boron concentration of 1465 ppm (i.e., the concentration making the colorset critical), instead of the value of 700 ppm used for two-group constant generation and for the nodal calculation.

We first want to verify whether the POD approach can accurately reproduce solutions used to build the original snapshot set. Therefore, we simulate the colorset in BRISINGR for one of the values of $N^{bp}_{B_{10}}$ spanned by the snapshot matrix (i.e., $9.3 \cdot 10^{-4}$ atoms/cm^3). For this configuration, Figure 3 reports a best-fit of the reference heterogeneous-assembly spectrum variation computed with the first four POD basis functions generated by the above-mentioned procedure. These are plotted in Figure 4. The quality of the fit is outstanding, despite of the low number of modes used. By comparing Figures 3 and 4 it is apparent that the first- and second-order POD basis retrieve the global shape of the reference spectrum deformation. The spiky profiles observable in the higher-order modes, especially in the epithermal region, contribute to the reconstruction of the fine details of $\delta\Phi(u)$, including those associated to the resonances (it is remarked that these spikes could be damped by generating snapshots with a deterministic transport code or using many more neutron histories). It can also be noticed that the computed modes inherit the property of the spectrum-variation snapshots to have null average within each macro-group, which is a consequence of the normalization introduced in Eq. (3). Thanks to this feature, we avoid defining discontinuous analytical basis functions when trying to fit the thermal-group spectrum change, whose values are very close to 0 in more than half of the corresponding pseudo-lethargy domain.

The spectrum variation estimated by the POD-based rehomogenization (calc. *c*) is plotted in Figure 5. The reconstruction is excellent in the thermal range, especially in the assembly hosting Pyrex rods. The prediction in the fast group is also accurate, though a slight overestimation of the magnitude of the reference change is observed in the epithermal region. Table I reports the results in terms of k_{eff} and average power for the nodal calculations *(a)*, *(b)* and *(c)*, whereas Table II shows the corresponding errors on nodal cross-sections for the two assemblies. Spectral corrections computed by rehomogenization reproduce almost exactly the reference ones in the thermal group. In the fast range, all corrections go in the right direction, apart from that for fast-to-thermal scattering (which has, on the other hand, a small contribution). The effectiveness of rehomogenization in improving the integral parameters is also apparent. The performance of the method is clearly not affected by the use of a set of POD basis generated at a considerably different diluted-boron concentration from the current one.

A brief analysis is now carried out on the behavior of the singular values of the fast- and thermal-group snapshot matrices A_1 and A_2 (see Section II.2.B). Figure 6 shows the singular values corresponding to four snapshot sets differing for their number: 50, 100, 150, 200. For all these sets, they decrease sharply for the first two modes in the thermal group and for the first three modes in the fast group, after which a sort of "plateau"

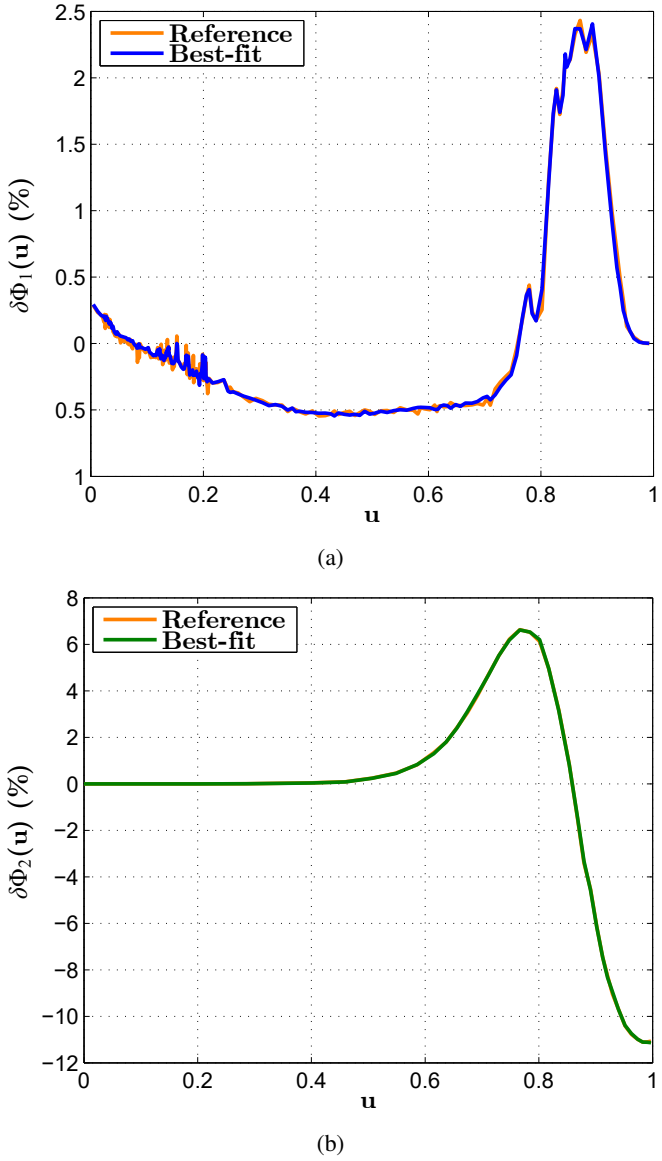

Fig. 3. POD fourth-order best-fit of the fast (a) and thermal (b) spectrum variation per unit lethargy for the assembly hosting Pyrex rods. The relative difference is computed with respect to the assembly-averaged integral fluxes from the reference calculation.

becomes apparent. This confirms that the very first low-order modes retain most of the information carried by the snapshot set, whereas a wide range of high-order modes has lower importance: these reproduce the finest details of the spectrum variation, but they do not contribute to reconstruct its global shape. It can also be observed that the first low-order singular values do not change significantly with the number of snapshots N_s, whereas those corresponding to higher-order modes (from the beginning of the "plateau" onwards) tend to increase with N_s. This behavior implies that, after an adequate number of snapshots, adding more of them (i.e., sampling more points in the parameter space) only results in a change of the lower sin-

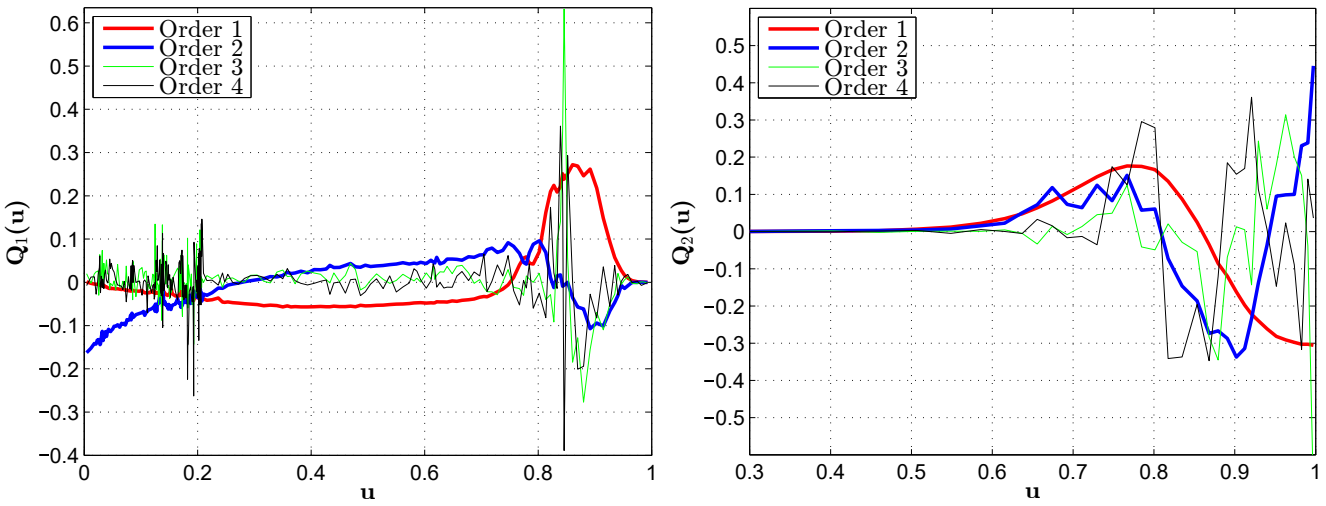

(a) (b)

Fig. 4. Fast-group (a) and thermal-group (b) POD basis functions computed via the method of snapshots and SVD for a one-parameter analysis of the colorset with Pyrex rods.

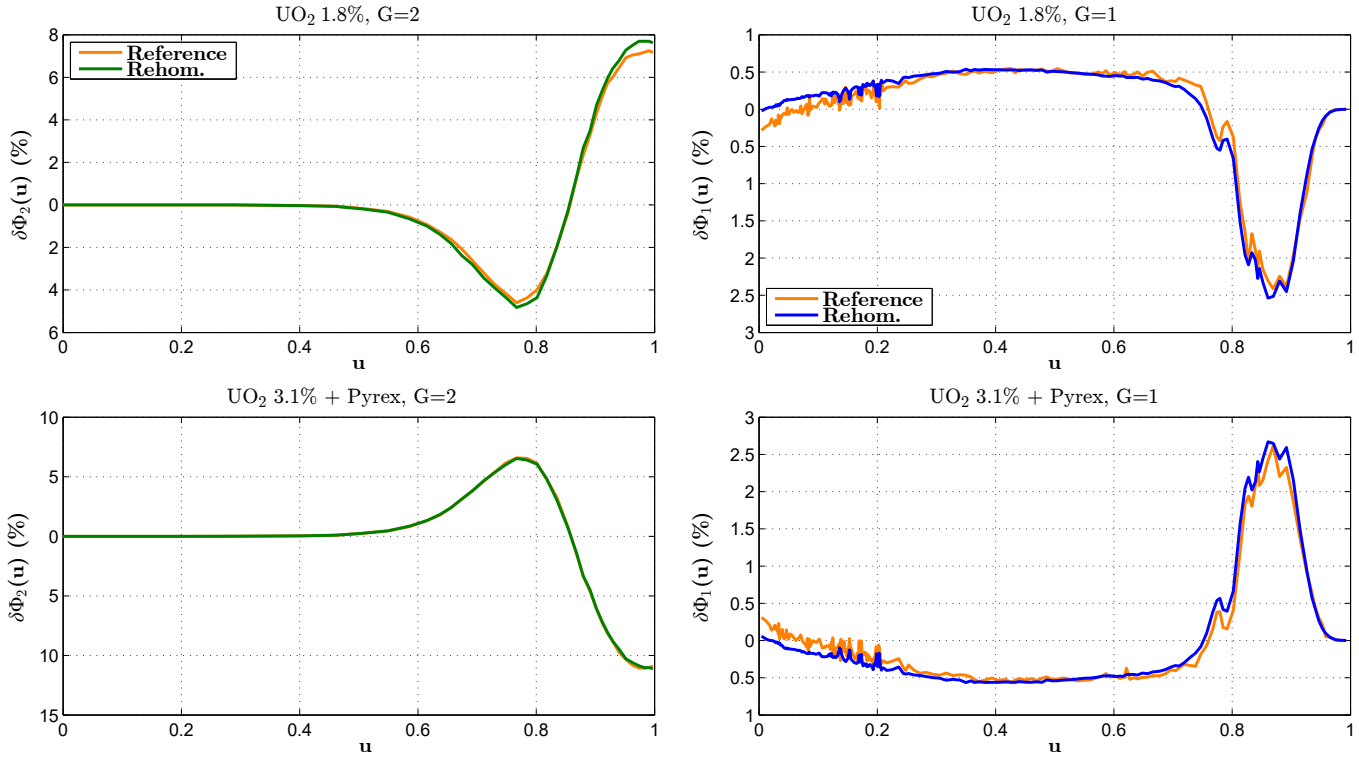

Fig. 5. Spectrum variation per unit lethargy estimated by the POD-based spectral rehomogenization in the two assemblies of the colorset with Pyrex rods (Figure 2). The relative difference is computed with respect to the assembly-averaged integral fluxes from the nodal calculation. Four modes were used in each coarse group for the modal expansion.

gular values, and does not affect the higher ones. Furthermore, these changes become less and less apparent as the number of snapshots increases. This feature is of paramount importance in the definition of a criterion for an adaptive selection of snapshots, which is, in a more general context, the subject matter of a companion paper at this conference [16].

An analysis of the singular-value behavior can thus give some relevant insight into the number of snapshots to be sampled

Table I. Errors on the multiplication factor (k_{eff}) and nodal fission power distribution (P_{avg}) for the colorset with Pyrex rods, having k_{eff}=1.08733. Power errors within brackets correspond to the fast (first value) and thermal (second value) groups. The number of rehomogenization iterations for convergence is also shown for simulation *(c)*.

			UO_2 1.8%	UO_2 3.1% + Pyrex
Simulation	No. rehom. iter	Δk_{eff} [pcm]	Error on P_{avg} (%)	Error on P_{avg} (%)
Standard (*a*)	-	-402	0.93 (0.82, 0.96)	-0.82 (-0.59, -0.89)
Ref. $\delta\Sigma^{spectr.}$ (*b*)	-	-372	0.43 (0.52, 0.42)	-0.38 (-0.37, -0.38)
Spectr. rehom. - POD (*c*)	8	-367	0.61 (0.62, 0.61)	-0.53 (-0.44, -0.56)

Table II. Errors (%) on nodal cross-sections for the assembly with 1.8% enrichment (a) and the one with 3.1% enrichment and burnable-absorber rods (b).

UO_2 1.8%	$\Sigma_{a,1}$	$\Sigma_{a,2}$	$\nu\Sigma_{f,1}$	$\nu\Sigma_{f,2}$	$\Sigma_{t,1}$	$\Sigma_{t,2}$	$\Sigma_{s,1\to1}$	$\Sigma_{s,1\to2}$	$\Sigma_{s,2\to1}$	$\Sigma_{s,2\to2}$
Reference [cm^{-1}]	0.00858	0.0621	0.00485	0.0825	0.539	1.310	0.513	0.0179	0.00124	1.246
Simulation	Error %									
Standard (*a*)	-0.251	0.747	0.396	0.838	-0.254	0.266	-0.268	0.124	-6.03	0.250
Ref. $\delta\Sigma^{spectr.}$ (*b*)	0.057	0.180	0.146	0.253	0.006	-0.053	0.006	0.003	0.038	-0.064
Spectr. rehom. - POD (*c*)	0.146	0.137	0.225	0.208	0.031	-0.078	0.019	0.308	0.36	-0.089

(a)

UO_2 3.1% + Pyrex	$\Sigma_{a,1}$	$\Sigma_{a,2}$	$\nu\Sigma_{f,1}$	$\nu\Sigma_{f,2}$	$\Sigma_{t,1}$	$\Sigma_{t,2}$	$\Sigma_{s,1\to1}$	$\Sigma_{s,1\to2}$	$\Sigma_{s,2\to1}$	$\Sigma_{s,2\to2}$
Reference [cm^{-1}]	0.00997	0.0978	0.00660	0.133	0.526	1.297	0.499	0.016	0.0017	1.198
Simulation	Error %									
Standard (*a*)	0.263	-0.496	-0.228	-1.11	0.254	-0.493	0.267	-0.166	6.76	-0.503
Ref. $\delta\Sigma^{spectr.}$ (*b*)	-0.021	0.328	-0.113	-0.219	-0.003	0.007	-0.003	0.002	-0.025	-0.019
Spectr. rehom. - POD (*c*)	-0.156	0.326	-0.210	-0.221	-0.045	0.005	-0.034	-0.327	-0.027	-0.021

(b)

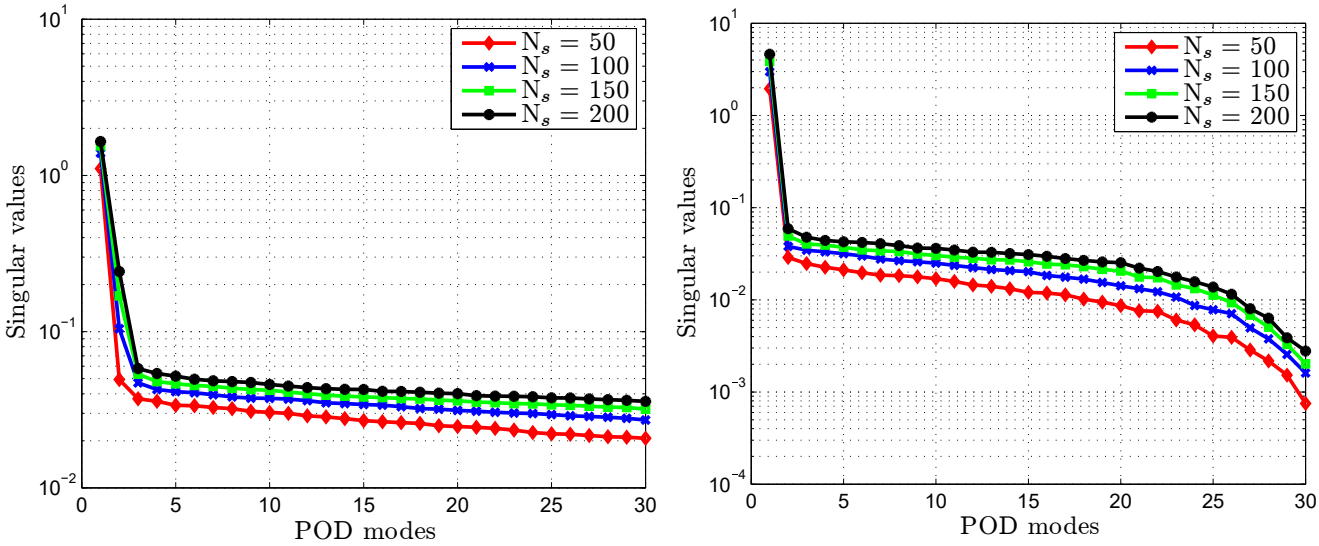

(a) (b)

Fig. 6. Singular values of the fast-group (a) and thermal-group (b) POD modes computed for the colorset with Pyrex rods. The dependence on the number of snapshots N_s is shown. Higher singular values correspond to low-order modes, whereas lower singular values correspond to high-order modes.

for the POD-basis calculation, as well as into the optimal number of modes to be used in the rehomogenization model for a sufficiently accurate approximation of the spectrum variation. It was verified that the precision of the results presented in

Tables I and II is not deteriorated either by the choice of POD basis generated from 50 snapshots (instead of 200) or by the use of two and three modes (instead of four) for the expansion of the thermal and fast spectrum variation, respectively.

B. Problem 2 - UO_2 Colorset with AIC Control Rods

We now increase the level of complexity of our analysis by performing a multi-parameter study for the generation of snapshots. We consider a colorset made of four 17×17 UO_2 assemblies with enrichment of 1.8%, two of which host 24 AIC (Silver-Indium-Cadmium) control rods. No boron is present in the moderator. The colorset- and assembly-layout is represented in Figure 7.

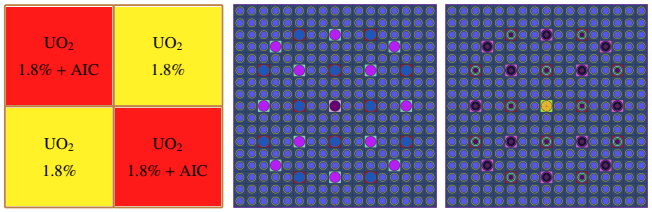

Fig. 7. Assembly set (a) and layout of the uncontrolled (b) and controlled (c) UO_2 fuel-assemblies with 1.8% enrichment.

In order to build a set of solutions representative of spectral effects induced by control elements and different enrichments, we parameterize the system using three variables:

- the fuel enrichment, which is homogeneously sampled in the interval [2.1%, 3.6%] for both the controlled and uncontrolled assemblies;
- the number of control rods inserted in each heterogeneous fuel bundle (4, 8, 12, 16, 24, 28), changed keeping the symmetry in the assembly layout;
- the type of control rods (AIC and B_4C).

A total number of 240 snapshots were computed. Moreover, we want to test the capability of the method to accurately predict spectrum deformations for "unseen" problems (i.e., problems whose solution was not included in the snapshot array for the determination of the POD basis). Therefore, we also apply spectral rehomogenization to the problem under study with the set of modes computed for the colorset with Pyrex. We refer to the nodal calculations with the AIC- and Pyrex-configuration sets of modes as *c1* and *c2*, respectively. The spectrum variation predicted in both cases is reported in Figure 8.
The set of POD basis from the multi-parameter analysis perfectly reconstructs the fast-group spectrum variation. A very accurate outcome is found also for the set of modes derived for the colorset with Pyrex, though a slight distortion of the computed distributions arises within the fast group in proximity of the high-energy "Maxwellian". As for the thermal group, no appreciable difference is encountered between the two calculations, for both of which the prediction is not as accurate as in the fast range (especially in the controlled assembly). The spectrum variation is indeed overestimated in the higher part of the thermal domain ($u \in [0.85,1.0]$) and underestimated in its intermediate region ($u \in [0.6,0.85]$). This misprediction might be related to the fact that in the thermal range most of the error is caused by spatial effects. In order to take them into account, spatial rehomogenization should thus follow the spectral correction.
Errors on integral parameters and nodal cross-sections are shown in Tables III and IV. The unexpectedly small error on k_{eff} for the standard calculation is the result of fortuitous error compensation, as evidenced by the high errors on the nodal power. The simulation with reference corrections still exhibits a somewhat high error on the thermal power, which confirms the need of applying spatial rehomogenization as well. When looking at errors on nodal cross-sections, the overestimation and underestimation of the spectrum change in different regions of the thermal domain cause some beneficial error cancellation in thermal absorption in both assemblies, as well as in production ($\nu\Sigma_f$) in the uncontrolled bundle.
It can be concluded that, also in this case, rehomogenization reproduces satisfactorily the calculation with reference corrections. In addition, the Pyrex modes can approximate the spectrum variation with a comparable accuracy to those computed "ad hoc" for controlled configurations.

C. Problem 3 - UO_2/MOX Colorset

The third colorset, which is shown in Figure 9, consists of two 18×18 UO_2 and MOX assemblies. The UO_2 assembly has enrichment 2.1%, whereas the MOX assembly is made of three fuel-pin types differing for their Pu-content and U-enrichment. The concentration of diluted boron in the moderator is 2907 ppm.
As for Problem 2, spectral rehomogenization was first applied with the POD modes computed for the Pyrex colorset (calc. *c1*). In this case, the basis functions resulting from high-order Legendre-polynomial best-fits of the original snapshots were used. This was done in order to eliminate the "noise" caused by a different pattern of the spectrum-change fine details in the two test-cases. Figure 10 shows the corresponding fast-group spectrum-variation reconstruction for the UO_2 assembly. Despite the accuracy of the outcome is acceptable in the epithermal range, it stands out that the method is not capable of recreating the "bump" observable at the end of the pseudo-lethargy domain (for $u \in [0.9,1.0]$). This is expected, as the POD basis computed for the Pyrex colorset were not "trained" to reproduce such localized, abruptly sign-changing bulge. This shape was found to be a characteristic of the present assembly-interface type, and to become even sharper when the enrichment in the UO_2 bundle is increased.
Rehomogenization was thus applied making use of two additional sets of basis functions (still using four modes in both groups):

- the POD modes obtained from a multi-parameter study for the present configuration, in which, following the example of Problems 1 and 2, the UO_2 enrichment and the Pu content in the three above-mentioned MOX-assembly pin types were considered as parametric variables;
- the POD modes obtained assembling all the snapshots computed for the three colorsets investigated in this study.

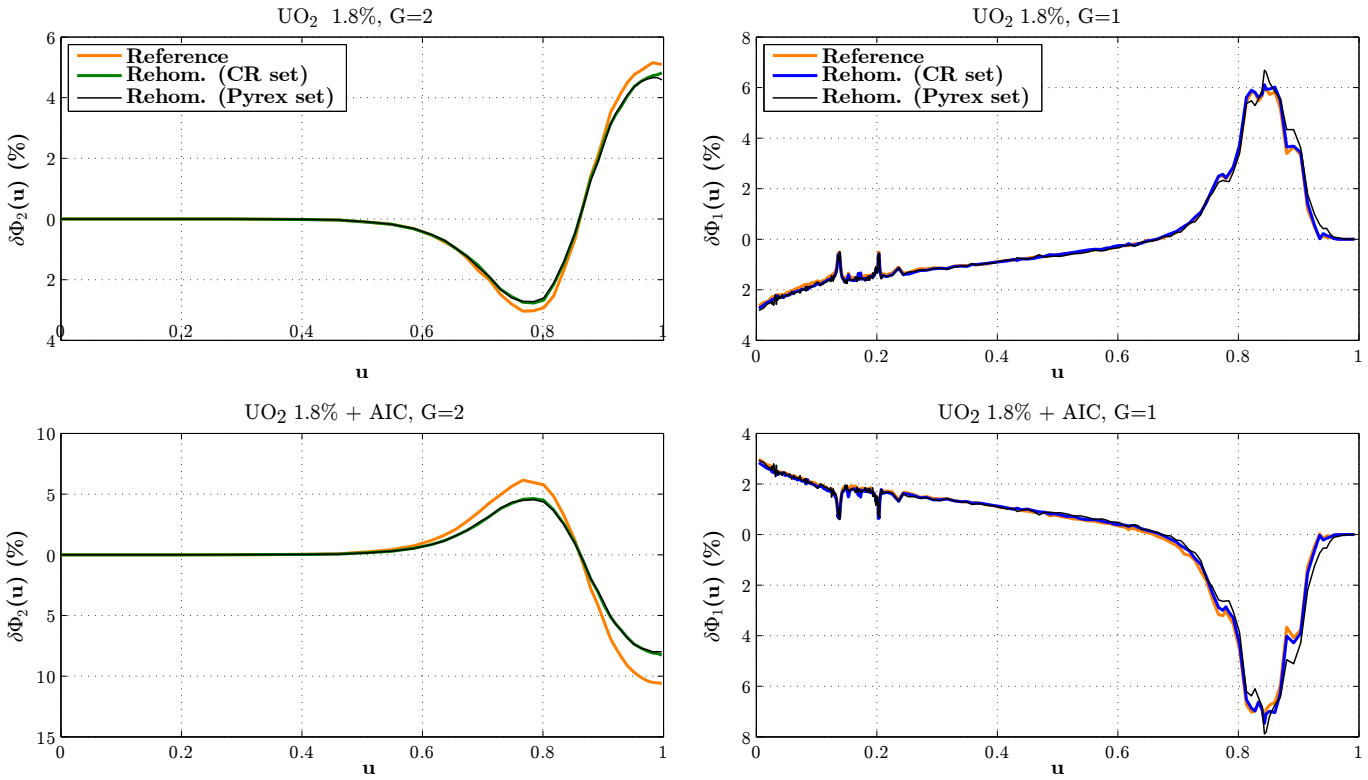

Fig. 8. Spectrum variation estimated by the POD-based rehomogenization in the two assemblies of the colorset with AIC control rods (Figure 7). Labels *Pyrex set* and *CR set* correspond to calculations *c1* and *c2*, respectively.

Table III. Errors on the multiplication factor (k_{eff}) and nodal fission power distribution (P_{avg}) for the colorset with control rods. For detailed meaning of *c1* and *c2*, see text. The reference value of k_{eff} is 0.98859.

			UO_2 1.8%	UO_2 1.8% + AIC
Simulation	No. rehom. iter	Δk_{eff} [pcm]	Error on P_{avg} (%)	Error on P_{avg} (%)
Standard (*a*)	-	54	3.07 (0.75, 3.50)	-4.77 (-0.89, -5.78)
Ref. $\delta\Sigma^{spectr.}$ (*b*)	-	-500	1.14 (0.22, 1.32)	-1.77 (-0.26, -2.18)
Spectr. rehom. - POD (*c1*)	8	-531	1.20 (0.27, 1.39)	-1.86 (-0.32, -2.29)
Spectr. rehom. - POD (*c2*)	9	-549	1.18 (0.36, 1.35)	-1.83 (-0.43, -2.22)

We refer to nodal simulations with these two sets of basis functions as *c2* and *c3*, respectively. The purpose of calculation *c3* is to verify whether rehomogenization combined with few low-order modes can still synthesize effectively spectral deformations triggered by different assembly-interface types, and thus exhibiting a considerably unlike behavior (especially in the fast range). This property of the POD modes is essential for the applicability of the proposed methodology at an industrial level, because it would allow us not to compute "fuel-dependent" modes.

Both calculations gave excellent results. As they were almost identical, for sake of conciseness we report them only for calculation *c3* (Figure 11, Tables V and VI).

Rehomogenization now manages to accurately reproduce the previously observed bulge in the fast group. Such outcome can be achieved only by a proper "training" of the POD modes, that is, if solutions for this particular assembly-configuration are included in the snapshot set. This feature can also be deduced from Figure 12, showing the fast-group POD basis computed from the snapshot set corresponding to calculation *c3*.

Apparently, the second-order mode retains the shape of the high-energy bulge, as well as the steep profile visible in the epithermal range (for $u \in [0,0.1]$) for the UO_2/MOX assemblies (see Figure 11). It must be remarked that merely analytical functions are unlikely to capture the strongly varying bulge-shape observed in the high-energy-part of the fast-group spectrum change, unless a very high order of the expansion is used. In the fast range, due to the fast fissions of U_{238} the production cross-section $\nu\Sigma_f(u)$ usually assumes its higher values for $u > 0.8$ (if one does not consider the resonance spikes).

Table IV. Errors (%) on nodal cross-sections for the assemblies without (a) and with (b) AIC control rods. For detailed meaning of *c1* and *c2*, see text.

UO_2 1.8%	$\Sigma_{a,1}$	$\Sigma_{a,2}$	$\nu\Sigma_{f,1}$	$\nu\Sigma_{f,2}$	$\Sigma_{t,1}$	$\Sigma_{t,2}$	$\Sigma_{s,1\to1}$	$\Sigma_{s,1\to2}$	$\Sigma_{s,2\to1}$	$\Sigma_{s,2\to2}$
Reference [cm^{-1}]	0.00827	0.0557	0.00486	0.0837	0.534	1.313	0.509	0.0174	0.0011	1.256
Simulation					Error %					
Standard (*a*)	1.59	0.562	0.492	0.608	0.680	0.155	0.558	3.80	-4.79	0.141
Ref. $\delta\Sigma^{spectr.}$ (*b*)	0.028	0.203	-0.135	0.237	-0.020	-0.047	-0.020	-0.051	0.0	-0.058
Spectr. rehom. - POD (*c1*)	-0.038	0.223	-0.150	0.258	-0.046	-0.036	-0.040	-0.219	-0.316	-0.047
Spectr. rehom. - POD (*c2*)	-0.068	0.227	-0.078	0.262	-0.073	-0.034	-0.066	-0.047	1.85	-0.146

(a)

UO_2 1.8% + AIC	$\Sigma_{a,1}$	$\Sigma_{a,2}$	$\nu\Sigma_{f,1}$	$\nu\Sigma_{f,2}$	$\Sigma_{t,1}$	$\Sigma_{t,2}$	$\Sigma_{s,1\to1}$	$\Sigma_{s,1\to2}$	$\Sigma_{s,2\to1}$	$\Sigma_{s,2\to2}$
Reference [cm^{-1}]	0.0116	0.0817	0.00474	0.0853	0.534	1.287	0.507	0.0153	0.00142	1.203
Simulation					Error %					
Standard (*a*)	-1.72	0.716	-0.641	-0.933	-0.806	-0.374	-0.665	-4.78	7.64	-0.457
Ref. $\delta\Sigma^{spectr.}$ (*b*)	0.596	1.28	0.199	-0.118	0.018	0.051	0.004	0.015	-0.011	-0.033
Spectr. rehom. - POD (*c1*)	0.517	1.14	0.083	-0.328	0.027	-0.059	0.017	-0.179	1.71	-0.143
Spectr. rehom. - POD (*c2*)	0.591	1.14	-0.024	-0.334	0.059	-0.062	0.050	-0.047	1.85	-0.146

(b)

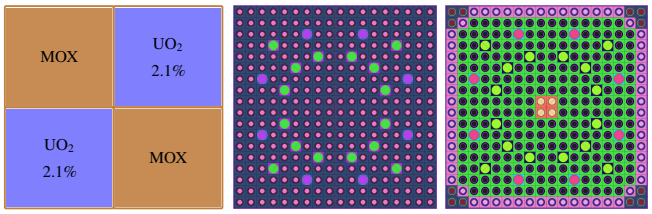

(a) (b) (c)

Fig. 9. Assembly set (a) and layout of UO_2 (b) and MOX (c) fuel-assemblies. Three different fuel-pin types are present in the MOX assembly: with low Pu-content (1.78% Pu_{239}, 0.22% U_{235}) at the assembly corners, with intermediate Pu-content (2.53% Pu_{239}, 0.21% U_{235}) along the assembly outer edges and with high Pu-content (3.86% Pu_{239}, 0.20% U_{235}) in the rest of the fuel bundle.

An accurate reconstruction of the spectrum deformation is thus needed also in this region of the energy domain to compute a reliable $\delta\nu\Sigma_f$, which significantly affects corrections on the integral parameters of the nodal calculation. This can be seen examining the errors on fast-group cross-sections (especially in the UO_2 assembly) and nodal power for calculation *c1*. Spectral rehomogenization with the POD basis of calculation *c3* was applied to Problems 1 and 2 as well. The corresponding results showed the same accuracy as the calculations with POD basis derived from parametric studies for the standalone colorsets.

3. Analysis on the State Parameters

We briefly consider here the impact of the main state parameters on the computed POD basis. We take as example

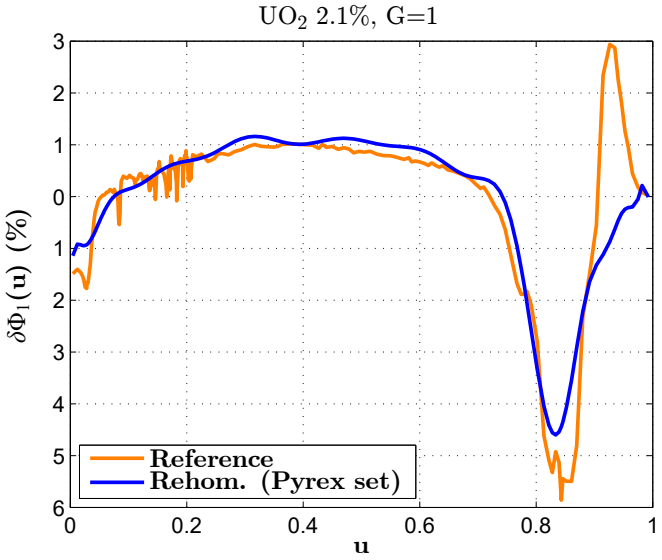

Fig. 10. Spectrum variation computed in the UO_2 assembly of the UO_2/MOX colorset (Figure 9) with the POD modes derived for the assembly set with Pyrex rods.

the colorset with Pyrex rods, for which previous results revealed that the performance of the POD-rehomogenization is not influenced by the value of diluted-boron concentration at which the snapshots are taken. Figure 13 represents the first-order POD modes determined sampling different points of the state-parameter space. The solid lines correspond to sets of snapshots at null burn-up and different values (with respect to the nominal conditions at which snapshot were generated in Section III.2.A) of diluted-boron concentration, moderator density and fuel temperature. The dashed lines correspond

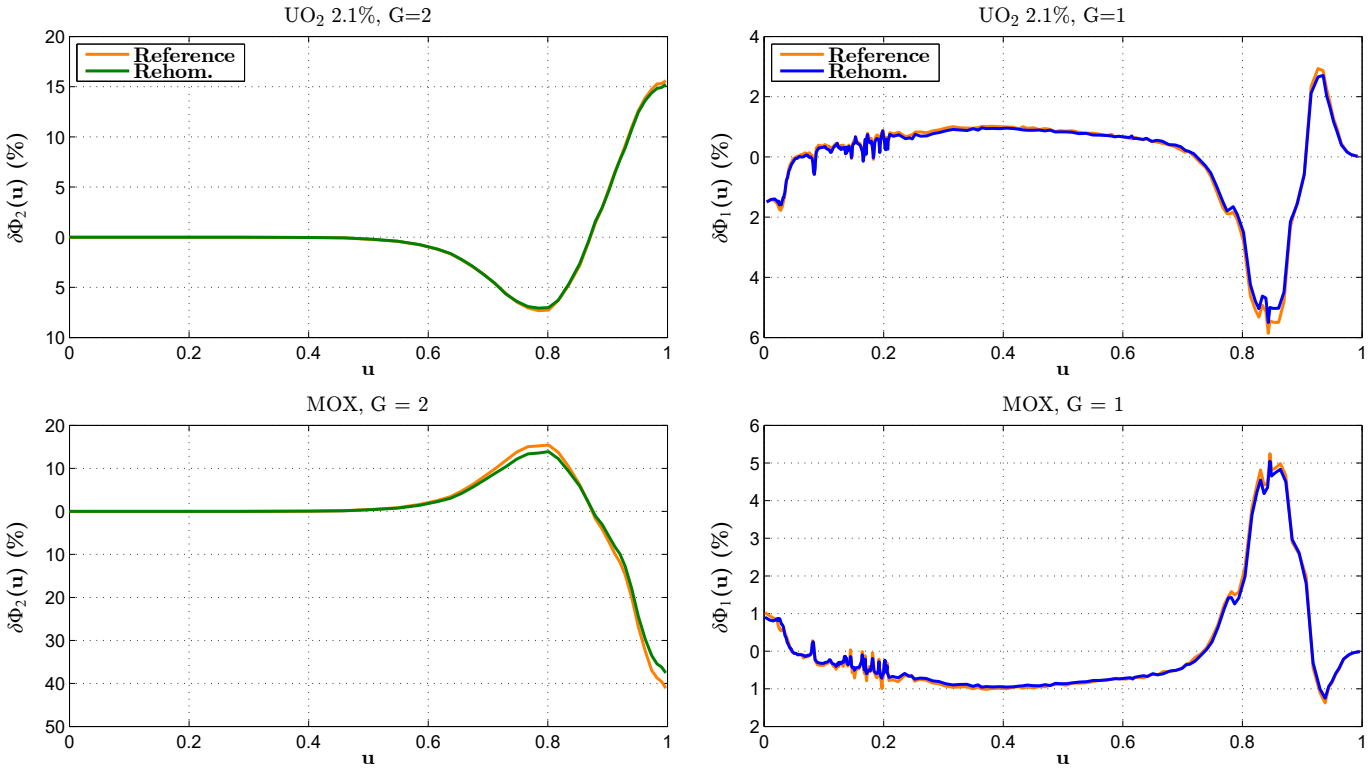

Fig. 11. Spectrum variation estimated by rehomogenization with the set of POD basis *c3*. The strong magnitude of the thermal-spectrum change in the MOX assembly is apparent.

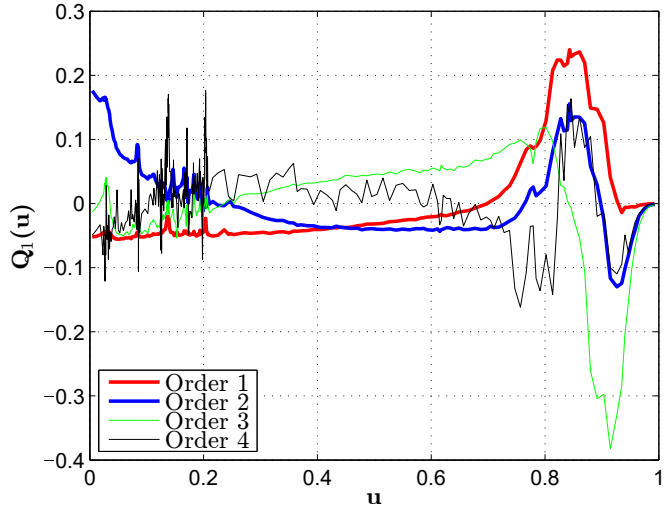

Fig. 12. Fast-group POD modes computed collecting all the snapshots simulated for Problems 1, 2 and 3.

instead to snapshots of the burn-up history of the colorset at the same nominal conditions. One hundred burn-up steps (up to 80 MWd/kgU) were considered to generate them. Apparently, for the thermal group the POD-basis shape does not depend on the state parameters. As for the fast group, the first-order basis also have a very much alike shape when considering snapshots computed for fresh fuel at different thermal and diluted-boron conditions. A similar outcome was found for the second- and third-order modes (which are not represented here for sake of brevity). However, more appreciable differences arise if solutions are sampled at different burn-up values. We found that these deviations become more apparent for higher-order modes. Such outcome is somewhat expected. It was observed, indeed, that the spectrum variation exhibits quite substantial changes as long as the fuel elements are burnt, both in its global shape and in its fine details. These differences are probably related to isotope build-up and, in the case considered here, to the depletion of burnable absorbers. Hence, the outcome of this preliminary analysis suggests that burn-up is the most significant state parameter to be sampled when building snapshots. Moreover, as the accumulation of Pu is usually strongly dependent on moderator conditions, it might be the case that also the coolant-related state parameters become important when generating snapshots for burn-up calculations.

4. A Model for the Leakage Energy Distribution

In the calculations performed so far the leakage energy distribution from the reference transport solution was used in the rehomogenization problem. In the final implementation of the methodology this shape has to be computed with nodal information. For this purpose, two tracks have been explored so far:

- a POD-basis expansion also for the leakage energy function $f_{L,G}(u)$ (Eq. (8a));

Table V. Errors (%) on nodal cross-sections for the UO_2 (a) and MOX (b) assemblies. For detailed meaning of *c1* and *c3*, see text.

UO_2 2.1%	$\Sigma_{a,1}$	$\Sigma_{a,2}$	$\nu\Sigma_{f,1}$	$\nu\Sigma_{f,2}$	$\Sigma_{t,1}$	$\Sigma_{t,2}$	$\Sigma_{s,1\to1}$	$\Sigma_{s,1\to2}$	$\Sigma_{s,2\to1}$	$\Sigma_{s,2\to2}$
Reference [cm^{-1}]	0.00927	0.0894	0.00547	0.0979	0.534	1.302	0.508	0.0171	0.00178	1.211
Simulation	Error %									
Standard (*a*)	-0.606	1.13	0.071	1.27	-0.326	0.536	-0.372	1.17	-8.89	0.507
Ref. $\delta\Sigma^{spectr.}$ (*b*)	0.114	0.185	0.365	0.301	0.011	0.017	0.011	-0.034	-0.058	0.005
Spectr. rehom. - POD (*c1*)	0.203	0.189	0.062	0.306	0.137	0.017	0.131	0.272	-2.08	0.006
Spectr. rehom. - POD (*c3*)	0.025	0.203	0.315	0.319	-0.014	0.027	-0.014	-0.054	-0.276	0.015

(a)

MOX	$\Sigma_{a,1}$	$\Sigma_{a,2}$	$\nu\Sigma_{f,1}$	$\nu\Sigma_{f,2}$	$\Sigma_{t,1}$	$\Sigma_{t,2}$	$\Sigma_{s,1\to1}$	$\Sigma_{s,1\to2}$	$\Sigma_{s,2\to1}$	$\Sigma_{s,2\to2}$
Reference [cm^{-1}]	0.0142	0.260	0.00990	0.375	0.526	1.517	0.498	0.0131	0.00345	1.254
Simulation	Error %									
Standard (*a*)	0.026	0.422	0.015	0.582	0.389	-0.651	0.432	-0.870	11.7	-0.908
Ref. $\delta\Sigma^{spectr.}$ (*b*)	-0.090	0.885	-0.254	1.08	-0.015	0.334	-0.014	0.035	-0.112	0.221
Spectr. rehom. - POD (*c1*)	-0.246	0.784	-0.271	0.958	-0.090	0.243	-0.086	-0.074	0.868	0.129
Spectr. rehom. - POD (*c3*)	-0.003	0.878	-0.254	1.08	0.004	0.239	0.004	0.024	0.917	0.105

(b)

Table VI. Errors on the multiplication factor (k_{eff}) and nodal fission power distribution (P_{avg}) for the UO_2/MOX colorset. For detailed meaning of *c1* and *c3*, see text. The reference value of k_{eff} for the colorset is 1.00196.

			UO_2 2.1%	MOX
Simulation	No. rehom. iter	Δk_{eff} [pcm]	Error on P_{avg} (%)	Error on P_{avg} (%)
Standard (*a*)	-	-85	1.85 (0.71, 2.19)	-1.39 (-0.41, -1.82)
Ref. $\delta\Sigma^{spectr.}$ (*b*)	-	-119	0.92 (0.99, 0.88)	-0.69 (-0.56, -0.73)
Spectr. rehom. - POD (*c1*)	8	-131	1.01 (0.77, 1.06)	-0.76 (-0.44, -0.88)
Spectr. rehom. - POD (*c3*)	7	-135	0.93 (0.97, 0.90)	-0.69 (-0.55, -0.74)

- a non-linear diffusive approach, in which the local leakage distribution is assumed to be proportional to the difference between the environmental spectrum in the node and the average environmental spectrum in the surrounding nodes.

The second strategy has given by far the best results, and is currently being investigated in detail. An example of its application, in combination with the POD approach for the trial/test functions, is shown in Figure 14 for the heterogeneous assembly of the colorset with Pyrex rods (Problem 1). The description of the new leakage model is deferred for subsequent publication, together with additional refinements of rehomogenization and a more extensive validation of the methodology.

IV. CONCLUSIONS

In this paper we showed that spectral rehomogenization, in conjunction with the POD-based approach for the search of basis/weighting functions, can reproduce very accurately core-environment effects associated to spectral interactions between fuel-assemblies when the reference-leakage energy distribution is used. Preliminary results of a leakage model using only nodal information are also very promising. It is therefore the authors' belief that the proposed methodology will contribute to obtain more accurate estimates of light-water-reactor power distribution and multiplication factor from nodal-diffusion codes, still using single-assembly-generated homogenization parameters. Our next challenge is the exploitation of the POD strategy at an industrial level. In order to capture as many characteristics as possible of the spectral interactions occurring in the reactor core and to find a set of rehomogenization modes effectively usable for several core layouts and states, a more extensive research of snapshots has to be performed. In our preliminary analysis we took advantage of the fact that spectrum deformations in the real environment often exhibit some common features regardless of the assembly-interface type, as well as a weak dependence on state parameters other than the burn-up. For a commercial-code target, a more systematic approach (possibly featuring adaptivity capability) is required, paying attention to minimize the computational burden of the off-line phase. For this purpose several sampling methods available in literature are currently being investigated.

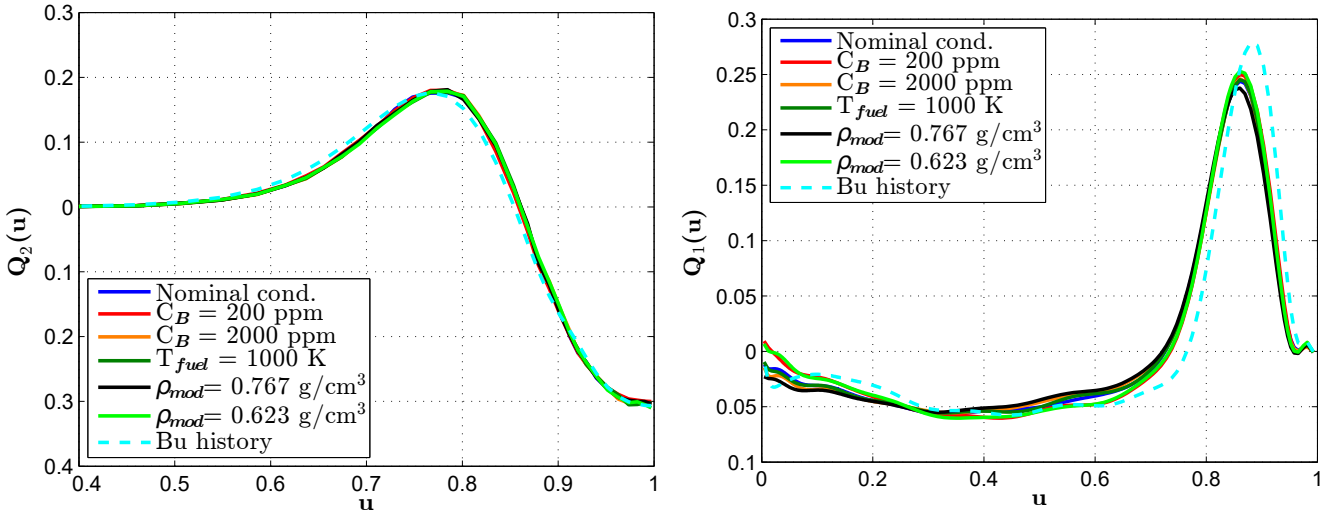

(a) (b)

Fig. 13. Thermal-group (a) and fast-group (b) POD modes computed for the colorset with Pyrex for different values of diluted-boron concentration (CB), fuel temperature (T_{fuel}), moderator density (ρ_{mod}) and burn-up (Bu). Nominal conditions correspond to CB=1465 ppm, T_{fuel}=846 K, ρ_{mod}= 0.708 g/cm^3. Burn-up snapshots (see dashed curves) were taken at these conditions.

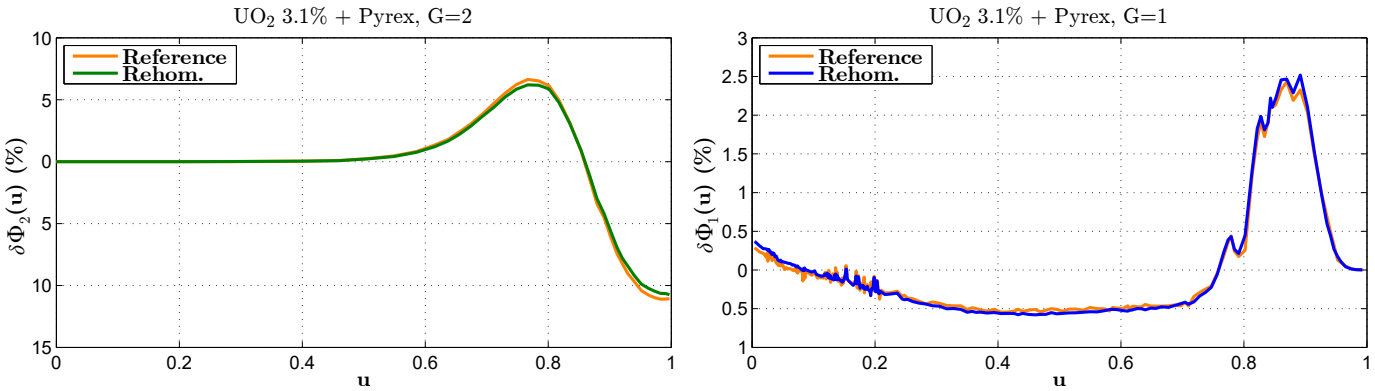

Fig. 14. Heterogeneous assembly of the colorset with Pyrex rods (Figure 2c): spectrum variation estimated by the POD-based rehomogenization, with a non-linear diffusive model for the leakage energy distribution using only nodal information and single-assembly data from cross-section libraries.

REFERENCES

1. K. S. SMITH, "Assembly homogenization techniques for Light Water Reactor analysis." *Progress in Nuclear Energy*, **17**, *3*, 303–335 (1986).
2. A. DALL'OSSO, "Spatial rehomogenization of cross sections and discontinuity factors for nodal calculations." in "Proc. of Int. Conf. PHYSOR," (2014).
3. S. PALMTAG and K. SMITH, "Two-group spectral corrections for MOX calculations." in "Proc. Int. Conf. Physics of Nucl. Sci. and Tech.", (1998), vol. 1, p. 3.
4. A. DALL'OSSO, D. TOMATIS, and Y. DU, "Improving Cross Sections via Spectral Rehomogenization." in "Proc. of Int. Conf. PHYSOR," (2010), pp. 9–14.
5. M. GAMARINO, D. TOMATIS, A. DALL'OSSO, D. LATHOUWERS, J. KLOOSTERMAN, and T. VAN DER HAGEN, "Investigation of Rehomogenization in the Framework of Nodal Cross Section Corrections." in "Proc. of Int. Conf. PHYSOR," (2016), pp. 3698–3707.
6. L. ZHU and B. FORGET, "An energy recondensation method using the discrete generalized multigroup energy expansion theory." *Annals of Nuclear Energy*, **38**, *8*, 1718–1727 (2011).
7. W. M. STACEY, *Modal approximations: theory and an application to reactor physics*, vol. 41, The MIT Press (1967).
8. A. CHATTERJEE, "An introduction to the proper orthogonal decomposition." *Current science*, **78**, *7*, 808–817 (2000).
9. K. KUNISCH and S. VOLKWEIN, "Galerkin proper orthogonal decomposition methods for parabolic problems."

Numerische mathematik, **90**, *1*, 117–148 (2001).

10. F. WOLS, *Transient analyses of accelerator driven systems using modal expansion techniques*, Master's thesis, Delft University of Technology (2010).
11. A. BUCHAN, C. PAIN, F. FANG, and I. NAVON, "A POD reduced-order model for eigenvalue problems with application to reactor physics." *International Journal for Numerical Methods in Engineering*, **95**, *12*, 1011–1032 (2013).
12. A. G. BUCHAN, A. CALLOO, M. G. GOFFIN, S. DARGAVILLE, F. FANG, C. C. PAIN, and I. M. NAVON, "A POD reduced order model for resolving angular direction in neutron/photon transport problems," *Journal of Computational Physics*, **296**, 138–157 (2015).
13. A. SARTORI, *Reduced order methods: applications to nuclear reactor core spatial dynamics*, Ph.D. thesis, Politecnico di Milano (2015).
14. L. SIROVICH, "Turbulence and the dynamics of coherent structures, part III: dynamics and scaling." *Quarterly of Applied mathematics*, **45**, 583–590 (1987).
15. J. LEPPÄNEN, M. PUSA, T. VIITANEN, V. VALTAVIRTA, and T. KALTIAISENAHO, "The Serpent Monte Carlo code: Status, development and applications in 2013," *Annals of Nuclear Energy*, **82**, 142–150 (2015).
16. F. ALSAYYARI, D. LATHOUWERS, and J. KLOOSTERMAN, "A non-intrusive POD approach for high dimensional problems using sparse grids." in "International Conference on Mathematics and Computational Methods Applied to Nuclear Science and Engineering (M&C 2017)," (2017).